

Osteoblasts derived from mouse mandible enhance tumor growth of prostate cancer more than osteoblasts derived from long bone



Matthew R. Eber^a, Sun H. Park^a, Kelly F. Contino^a, Chirayu M. Patel^a, Fang-Chi Hsu^b, Yusuke Shiozawa^{a,*}

^a Department of Cancer Biology and Wake Forest Baptist Comprehensive Cancer Center, Wake Forest University Health Sciences, Winston-Salem, NC 27157, USA

^b Department of Biostatistics and Data Science and Wake Forest Baptist Comprehensive Cancer Center, Wake Forest University Health Sciences, Winston-Salem, NC 27157, USA

ARTICLE INFO

Article history:

Received 6 May 2020

Revised 12 December 2020

Accepted 14 December 2020

Keywords:

Prostate cancer

Osteoblasts

Mandible osteoblasts

Hind limb osteoblasts

Bone metastasis

Tumor cell proliferation

ABSTRACT

Prostate cancer (PCa) metastasizes to bone, where the bone marrow microenvironment controls disease progression. However, the cellular interactions that result in active bone marrow metastases are poorly understood. A better understanding of these interactions is critical to success in the pursuit of effective treatments for this life ending disease. Anecdotally, we observe that after intracardiac injection of PCa cells, one of the greatest tools to investigate the mechanisms of bone-metastatic disease, animals frequently present with mandible metastasis before hind limb metastasis. Therefore, in this study, we investigated whether the bone cells derived from the mouse mandible influence PCa progression differently than those from the hind limb. Interestingly, we found that osteoblasts harvested from mouse mandibles grew faster, expressed more vascular endothelial growth factor (VEGF), increased vascularity and formed more bone, and stimulated faster growth of PCa cells when cultured together than osteoblasts harvested from mouse hind limbs. Additionally, these findings were confirmed *in vivo* when mouse mandible osteoblasts were co-implanted into mice with PCa cells. Importantly, the enhancement of PCa growth mediated by mandible osteoblasts was not shown to be due to their differentiation or proliferation activities, but may be partly due to increased vascularization and expression of VEGF.

© 2020 The Author(s). Published by Elsevier GmbH. This is an open access article under the CC BY-NC-ND license (<http://creativecommons.org/licenses/by-nc-nd/4.0/>).

1. Introduction

Prostate cancer (PCa) is deadly when it metastasizes to bone, often years after a patient is cured of the primary disease. These metastases are believed to originate from disseminated tumor cells (DTCs) shed from the primary tumor that made their way to the bone marrow and became dormant. Once in the bone marrow, progression of dormant DTCs in the bone is directed by influences from the bone marrow microenvironment. Still, a full understanding of the more complex interactions that result in active bone marrow metastases remains elusive. Our group recently discovered that early in the metastatic process, PCa cells target and commandeer the hematopoietic stem cell (HSC) specific marrow microenvironment, or HSC niche, using mechanisms similar to those involved in HSC homing to bone [1]. Osteoblasts are a major component of the HSC niche and have been shown to participate in the regulation of HSC homing and quiescence (or dormancy) [2–5]. Interestingly, DTCs also utilize osteoblasts to establish early colonization within the marrow [1,6]. Thereafter, the DTCs lie dormant

within the osteoblastic niche until they begin to proliferate again, controlled by mechanisms still poorly understood, and eventually develop into full-blown metastases [7].

A tool frequently used to investigate the mechanisms of metastasis is the intracardiac injection mouse model. After a small volume of cancer cells is inoculated into the left ventricle of the mouse heart, the circulatory system becomes flooded with cancer cells that eventually colonize organs of preference, such as bone. As expected, this model consistently results in long bone metastases, including lesions in the femur and tibia. However, mandible metastases are also frequently observed in this model [8]. This appears to be a phenomenon unique to this model, as metastasis to the human mandible is uncommon for solid tumors known to metastasize to the bone, such as PCa [9]. Anecdotally, using this model we have found that sometimes the only site of metastasis is the mandible, and that in animals with multiple bone metastatic lesions, many demonstrate faster growth in the mandible than those in the hind limbs of the same animal (unpublished observations). These findings raise the question whether the bone marrow microenvironment of the mandible stimulates the growth of DTCs more than that of the hind limbs. One difference between bone cells derived from mandible and long bones that has been documented is their proliferative and differentiation potential. Indeed,

* Corresponding author at: Department of Cancer Biology, Wake Forest University Health Sciences, Medical Center Blvd., Winston-Salem, NC 27157-1082, USA.
E-mail address: yshiozaw@wakehealth.edu (Y. Shiozawa).

osteoblasts derived from rat mandible bone marrow grew faster and formed more bone *in vivo* than those differentiated from long bone marrow [10]. The same effects were seen in human tissue cultures of mandible and iliac marrow derived osteoblasts [11]. Interestingly, it has recently been revealed that different subpopulations of osteoblasts contribute differently to bone metastatic progression [12]. Therefore, we hypothesized that osteoblasts harvested from mouse mandible bones would enhance the growth of PCa cells when they interact with each other, more than those harvested from hind limb bones.

In this study, we found that osteoblasts harvested from mouse mandible bones grew faster than those harvested from hind limb bones, similar to the reports of osteoblasts derived from rat and human tissues. Additionally, osteoblasts harvested from mouse mandibles expressed higher levels of vascular endothelial growth factor (VEGF). Moreover, when these osteoblasts were cocultured with PCa cells, osteoblasts harvested from mouse mandibles significantly increased the growth of PCa cells compared to osteoblasts harvested from hind limbs. Most importantly, these findings were confirmed *in vivo*, and immunofluorescent staining of pathological specimens revealed that vascularity of mandible osteoblast implants was greater than hind limb osteoblast implants.

2. Materials and methods

2.1. Cell culture

Human PCa cell line PC-3 [American Type Culture Collection (ATCC), Manassas, VA, Cat #: CRL-1435] and DU145 cells (ATCC, Cat #: HTB-81) were transformed to stably express green fluorescent protein (GFP) and firefly luciferase (PC3-GFP-luc, and DU145-GFP-luc) by transduction with a lentivirus (Lenti-GF1-CMV-VSVG) generated by the University of Michigan Vector Core. The transduced cells were sorted for GFP positive cells at the Wake Forest Baptist Comprehensive Cancer Center Flow Cytometry Shared Resource using an Astrios EQ (Beckman Coulter, Pasadena, CA), expanded and frozen at low passage (<10). The growth media for PC-3 and DU145 was RPMI 1640 (Gibco, Gaithersburg, MD, Cat #: 11875093) supplemented with 10% FBS (Sigma-Aldrich, St. Louis, MO, Cat #: F2442), 1% Penicillin-Streptomycin (Gibco, Cat #: 15140122), and 1% L-Glutamine (Gibco, Cat #: 25030081). Murine calvarial pre-osteoblast cell line MC3T3-E1 Subclone 4 (ATCC, Cat #: CRL-2593) were cultured with MEM α without nucleosides (Gibco, Cat #: 12561056) supplemented with 10% FBS, 1% Penicillin-Streptomycin, and 1% L-Glutamine. Before supplementation, this formulation of MEM α already contains 50 mg/L Ascorbic Acid, and therefore no additional Ascorbic Acid was required. Cells were incubated at 37°C, 5% CO₂, and 100% humidity and were routinely passaged when no more than 80% confluent.

2.2. Animal care and use certification

All animal studies were approved by the Institutional Animal Care and Use Committee (Protocol A18-036) at Wake Forest University Health Sciences.

2.3. Intracardiac PCa inoculation and imaging of tumor growth

DU145-GFP-Luc (1×10^6 cells/100 μ L of PBS) cells were injected into immunocompromised Athymic Nude mice (Charles River Laboratories, Wilmington, MA, Cat #: 490) by left ventricular intracardiac injection, as previously described [13]. To monitor cancer growth, luciferase signal was followed at least once a week for

10 weeks using the IVIS Lumina Series III system and Living Image software (Xenogen, Alameda, CA).

2.4. Primary murine osteoblast culture

Hind limbs and mandibles were dissected from 5-week old male C57BL6/J mice (The Jackson Laboratory, Bar Harbor, ME, Cat #: 000664). Epiphyses from the femurs and tibias were cut and the marrow was removed by centrifugation, as previously described [14]. Briefly, an 18g hole was bored into the bottom of a 0.6 mL microcentrifuge tube with a needle, and then the tube was placed in a 1.7 mL microcentrifuge tube. The diaphyses of the bones were placed in the smaller tube, and the apparatus was then centrifuged at max speed for 30 sec. Afterward, the bone fragments remained in the upper 0.6 mL tube, and the marrow was pelleted in the bottom 1.7 mL tube. The empty diaphyses were placed into a 10 cm dish in HBSS, no calcium, no magnesium, no phenol red (Gibco, Cat #: 14175095) supplemented with 1% Penicillin-Streptomycin and minced into smaller pieces using a scalpel. The molars, incisors and dental pulp of the mandibles were removed and the remaining pieces (ascending ramus containing the coronoid, condylar and angular processes) were placed into a 10 cm dish in HBSS supplemented with 1% Penicillin-Streptomycin and minced into smaller pieces using a scalpel. After forceful washing to remove all marrow, a 10 min Trypsin-EDTA digestion was performed on the bone and mandible pieces at 37°C. Complete MEM α [MEM α without nucleosides supplemented with 10% FBS, 1% Penicillin-Streptomycin, 1% L-Glutamine, and 10nM dexamethasone (Sigma-Aldrich, Cat #: D4902) [15]] was then added to the explant cultures and the mature bone cells were allowed to migrate out of the bone and mandible pieces and expand for two weeks. In some cases, the cells were grown in bone mineralization medium (BMM) to induce further osteoblastic differentiation and mineral deposition: this media is complete MEM α supplemented with 0.5mM L-Ascorbic acid (Sigma, Cat #: A5960), 2mM β -Glycerophosphate disodium salt hydrate (Sigma-Aldrich, Cat #: G9422), and 10mM HEPES (Thermo Fisher Scientific, Hampton, NH, Cat #: BP299). The control media for BMM is complete MEM α supplemented with 10mM HEPES (vehicle).

2.5. MTT assay

Cells were seeded at a density of 4×10^3 cells/100 μ L complete MEM α into each well of a 96-well plate and incubated for 1, 3, and 5 days. To measure relative cell numbers, 500 μ g/mL MTT (Tocris Bioscience, Minneapolis, MN, Cat #: 5224) was added to each well and incubated for 4 h. The reaction was halted, and the formazan precipitate was dissolved by the addition of an equal volume of 10% SDS in 0.01 M HCl (10 g/100 mL). The plate was incubated at 37°C, 5% CO₂, and 100% humidity overnight and read on a plate reader at 560 nm with a background measurement at 650 nm.

2.6. In vitro mineralization assay

Cells were seeded at a density of 1×10^5 cells/250 μ L complete MEM α into each well of a 24-well plate and incubated for 24 h. The complete MEM α was then replaced with 500 μ L fresh complete MEM α and the plate was incubated for 48 h. The media was replaced with vehicle or BMM and incubated for 72 h. This process was continued every other day for a total of 14 days from first treatment. Half of the wells were harvested for mRNA. The remaining wells were stained with Alizarin Red S (ARS) to quantify total mineralization. Briefly, cells were fixed with 10% neutral buffered formalin for 5 min at room temperature and then stained with 2% ARS (Sigma-Aldrich, Cat #: A5533-25G) at pH 4.1 in water (2 g/100 mL) for 30 min at room temperature. Excess stain was

washed out in running tap water until the water ran clear. Representative images were captured on an EVOS inverted microscope (Thermo Fisher Scientific). Stain from each wells was quantified after lysing entire contents as described elsewhere using an acetic acid extraction method and plate reader absorbance at 405 nm [16].

2.7. Real Time qPCR

Confluent and multilayered osteoblastic cells were lysed, and RNA was harvested using the RNeasy Plus Mini Kit (Qiagen, Germantown, MD, Cat#: 74134). The RNA concentrations were determined and subsequently normalized between samples prior to cDNA generation using Invitrogen SuperScript II Reverse Transcriptase (Invitrogen, Carlsbad, CA, Cat#: 18064022). Real time qPCR was performed using TaqMan Gene Expression Master Mix (Applied Biosystems, Foster City, CA Cat#: 4369016) and Taqman Gene Expression Assays [Applied Biosystems, Cat#: 4331182, Assay IDs: Mm03413826_mH (*Bglap*: Osteocalcin, OCN), Mm00436767_m1 (*Spp1*: Osteopontin, OPN), Mm00437306_m1 (*Vegfa*: vascular endothelial growth factor, VEGF), Mm00441906_m1 (*Tnfrsf11*: RANKL), Mm00435454_m1 (*Tnfrsf11b*: Osteoprotegerin, OPG), Hs00921372_m1 (*TNFRSF1*: RANK), Hs02786624_g1 (*GAPDH*), and Mm99999915_g1 (*Gapdh*)] on the Bio-Rad CFX Connect instrument (Hercules, CA). Data is presented as relative gene expression using the delta-delta Ct method, with *Gapdh* used as the reference gene.

2.8. Co-culture assay

Primary cells, or MC3T3-E1 cells, were seeded at a density of 2×10^4 cells/100 μ L complete MEM α into each well of a 96-well plate and incubated for 24 h. In some cases, cells were growth arrested for 2.5 h with 10 μ g/mL mitomycin-C (Sigma-Aldrich, Cat #: 10107409001). Thereafter, cancer cells were seeded on top of the bone cells or by themselves in new 96-well plates, at a density of 2×10^3 cells/100 μ L complete MEM α . Plates were incubated for 48 h and the media replaced with vehicle or BMM, and incubated for 1, 3, and 5 days, with media replacement at each time point. To monitor cancer growth in real time, luciferase signal was checked before each media replacement using the IVIS system, after addition of 200 μ g/mL D-Luciferin (PerkinElmer, Waltham, MA, Cat #:122799) and 10 min incubation at 37°C.

2.9. Ossicle implantation

1×10^5 DU145-GFP-luc and/or 1×10^6 primary cells [mandible osteoblasts (MaOBs) or hind limb osteoblasts (HLOBs)] were suspended in 10 μ L BMM in individual microcentrifuge tubes (inoculum tube) and stored on ice until implantation. Under sterile conditions, absorbable gelatin sponges (Ethicon, Somerville, NJ, Cat #: 1973) were cut into small cubes (~ 5 mm³) and placed in a petri dish containing BMM on ice until implantation. Mice were anesthetized, backs shaved if necessary, and the surgical site was prepared using betadine. Blunt tipped scissors were used to create a small incision (~ 1 cm) in the dorsal skin parallel to the spine, and the scissors were used to create subcutaneous pouches on both sides of the incision. Using fine tipped forceps, a sponge piece was removed from the petri dish, excess liquid was blotted using sterile gauze, and then seeded by placing it in the bottom of an inoculum tube and allowing it to absorb the entire inoculum. The seeded sponge was then implanted into one of the subcutaneous pouches. Each animal received an implant seeded with HLOBs in one pouch and an implant with MaOBs in the opposite pouch. The incision was closed with surgical staples, which were removed after 7 days. Animals implanted with tumor seeded cells were

athymic nude mice and animals implanted with only primary cells were C57BL6/J (male, 5 weeks old). In order to monitor cancer growth in co-culture seeded ossicles *in vivo*, luciferase signal was followed at least once a week for 20 weeks using the IVIS system, whereas primary cell only seeded ossicles were grown for 7 weeks *in vivo*.

2.10. Tissue processing

After euthanasia, the implants were dissected and placed in 10% neutral buffered formalin for 24 h at 4°C under agitation. They were then radiographed using the MultiFocus 10x15 Digital Radiography System (Faxitron Bioptics, Tucson, AZ). Radiographs were analyzed using ImageJ software (NIH, Bethesda, MD) for densitometry. Briefly, tissue was outlined using the freehand tool and Max Gray values were determined for each implant. Next, the implants were placed in cassettes and decalcified for 14 days in 10% ethylenediaminetetraacetic acid (EDTA), with fresh solutions replaced on day 7. The tissues were then cryopreserved in 30% sucrose for 48 h. They were halved with a razor blade and one half of each tissue was arranged in plastic molds containing optimal cutting temperature (OCT) media and frozen on dry ice. Using a cryostat, 10 and 20 μ m sections were made and stored at -80°C . The other tissue halves were processed for paraffin embedding and sectioned on a microtome at 5 μ m sections. Hematoxylin and Eosin (H&E) staining was performed on sections, as well as immunohistochemistry (IHC) for Ki67 (Abcam, Cambridge, MA, Cat#: ab16667), and immunofluorescence (IF) for Osteocalcin (Takara Bio USA, Mountain View, CA, Cat#: M173), Pancytokeratin (Novus Biologicals, Centennial, CO, Cat #: NB600-579SS), Endomucin (Santa Cruz Biotechnology, Dallas, TX, Cat#: sc-65496), VEGF (Santa Cruz Biotechnology, Cat#: sc-7269), and CD31 (R&D Systems, Minneapolis, MN, Cat #: AF3628) as previously described [17]. Antigen retrieval was performed using Biogenex DeCal Retrieval Solution (Biogenex, San Ramon, CA, Cat#: HK089-5K) before incubating with the primary antibody at a concentration of 1:500 overnight at 4°C. Sections were then labeled with secondary rabbit antibody (Biogenex, Cat#: HK336-5R), Vectastain Elite ABC HRP kit (Vector, Burlingame, CA, Cat#: PK-6100) and DAB Peroxidase (HRP) Substrate Kit (Vector, Cat#: SK-4100). Slides were mounted in permanent mounting media and scanned on a NanoZoomer slide scanner (Hamamatsu, Japan) at 40x magnification. Quantitative analysis was performed using Visiopharm software (Westminster, CO) and an APP designed to automatically count DAB and hematoxylin alone positive nuclei, as well as determine tissue section area on the entire slide.

2.11. Statistical analysis

Metastatic tumor growth was measured by bioluminescent imaging (BLI), and radiance values were log transformed in order to satisfy the conditional normality assumption. The mean and standard error of the mean (SEM) of log transformed radiance values were calculated by time and location of metastatic lesions (mandible vs. hind limb). For exploratory purposes, comparisons of log transformed radiance values between locations at each time point were performed using the paired Student's t-tests. Mean differences in log transformed radiance between locations were also estimated using the mixed effects model with time, location, and interaction between time and location included in the model. The advantage of using this model was that all data were analyzed simultaneously, resulting in more efficient estimates. The hypothesis test for location effect at each time point was performed using a contrast. The nested (location within each mouse) random intercepts were used to take into account the correlated structure (e.g., repeated measures over time; measures at different locations in

the same mouse). Sub-analysis of the same data was performed to compare metastasis-free survivals, as measured with a 75% signal cut off. Event time was defined as the time from the beginning of the study to the initial endpoint (\geq the 75th percentile of log transformed radiance) and censoring time as the time from the beginning of the study to the last assessment or death. The Kaplan-Meier survival curves for the initial endpoint by location were plotted. The comparison between the two survival curves were performed using the Cox proportional hazards model with robust sandwich estimates to take into account the correlated structure (e.g., different locations in the same mouse). The same statistical approaches were applied to analyses of tumors co-cultured with primary cells (MaOBs or HLOBs).

The distributions for the other outcome measures such as gene expression and OD were confirmed to be normal. The means and SEM of the outcome measures were calculated by tissue origin (mandible vs. hind limb) and by treatment (vehicle vs. BMM), and comparisons of the outcome measures were performed using the unpaired Student's t-test. The means and standard errors of the tissue section areas and of MaOB or HLOB ossicles were calculated and compared using the paired Student's t-test.

The comparison of log transformed average radiance between the combination of primary cells (MaOBs vs. HLOBs) and treatment (vehicle vs. BMM) at each time point was performed using the analysis of variance (ANOVA) for exploratory purpose. Mean differences in log transformed radiance between primary cells and treatments at each time point were also estimated using the mixed effects model with time, location, treatment, and two-way and three-way interactions included in the model. If higher order interactions were not statistically significant, they were removed from the model. For PC3 co-culture analyses, the interaction between primary cells and time as well as the interaction between treatment and time were included in the model. For DU145 co-culture analyses, only the interaction between primary cells and time was included in the model. The random intercept was used to handle repeated measurements over time. The hypothesis tests for primary cell effect and BMM effect at each time point were performed using contrasts. All the analyses were performed using the GraphPad Prism statistical program (GraphPad Software, San Diego, CA) and the SAS software (SAS Inc, Cary, NC) with significance at $P \leq 0.05$.

3. Results

3.1. Intracardiac injection results in lesions in the mandibles before the hind limbs.

Since we have anecdotally found that mandible metastases occur faster than hind limb metastases in mice following intracardiac injection of PCa cells, we sought to examine more detailed metastatic patterns and tumor growth capacities of PCa cells in the intracardiac model. To do so, human PCa cell line DU145-GFP-luc cells were inoculated intracardially into immunocompromised athymic nude mice. When the bioluminescent imaging (BLI) signals of nude mice inoculated with DU145-GFP-luc were followed, detectable tumors in the mandibles were significantly brighter, and therefore larger in size than those in the hindlimbs at day 29, but over time signals at both sites became similar (Fig. 1A&B). Curiously, the BLI signals of the mandibles actually begin to decrease after day 29, which might be explained by tumor necrosis or hypoxic environments associated with fast-growing tumors [18]. Sub-analysis of the same data was performed to compare metastasis-free survivals, as measured with a 75% signal cut off, and the onset of metastasis in the mandible appeared to occur

sooner than the hindlimb, although not statistically significant (Fig. 1C).

3.2. Cells derived from mandible and hind limb bone explants have osteoblastic characteristics.

To dissect out the differences between cells in the mandibles and hind limbs, we decided to compare the functions of osteoblasts from these two areas, since proliferation of PCa is known to be regulated in part by osteoblasts [19–21]. After cleared of soft tissue and bone marrow, bone pieces obtained from the mandibles and hind limbs (femurs and tibias) of adult C57BL6/J mice were minced (Fig. 2A) and cultured in media containing dexamethasone (10nM) to differentiate any remaining cells into osteoblasts [15]. After two weeks of culture, cells derived from the bone explants were assessed of their osteoblastic characteristics. Both cultures expressed relatively high levels of the osteoblastic markers Osteocalcin and Osteopontin (Fig. 2B&C). Basal expression of Osteocalcin and Osteopontin were both lower in the mandible cell cultures than the hind limb cultures, but the presence of both markers in vehicle-treated cells revealed that the cultured bone explant cells are mostly differentiated even without the use of differentiation supplements, unlike traditional bone marrow stromal cell culture preps (Fig. 2B&C). After treatment with known osteoblastic differentiation supplements L-Ascorbic acid and β -Glycerophosphate, the levels of these markers were significantly increased in both explant cultures, however cultures of mandible cells responded to L-Ascorbic acid and β -Glycerophosphate to a greater degree than cultures of hind limb cells (Fig. 2B&C). As vascular endothelial growth factor (VEGF) derived from osteoblasts, encoded by the mouse gene *Vegfa*, has been shown to be involved in osteoblast differentiation and mineralization [22], and VEGF is implicated in PCa migration to bone and growth through induction of angiogenesis [23], we tested whether *Vegfa* expression was increased in mandible cultures. Basal expression of *Vegfa* was higher in cultures of mandible cells than those of hind limb cells and was not significantly changed in response to L-Ascorbic acid and β -Glycerophosphate supplementation in either mandible or hind limb cultures (Fig. 2D). To further test osteoblastic functional capabilities, the mineralization potentials of these cells were evaluated using Alizarin Red S (ARS) staining. Both cells derived from mandible and hind limb explants were able to mineralize, as evidenced by ARS staining (Fig. 3A&B). Interestingly, cells from mandible explants showed more mineralization than cells from hind limb explants, regardless of L-Ascorbic acid and β -Glycerophosphate supplementation (Fig. 3B). We attribute this observation to the previous finding that differentiation supplements were not required for osteoblast marker expression in our bone explant cultures (Fig. 2B&C), and therefore, not required for mineralization either. Altogether, this suggests that the cells derived from mandible and hind limb bone explants have osteoblastic characteristics. Therefore, from here on, the cells derived from mandible and hind limb bone explants will be referred to as mandible osteoblasts (MaOBs) and hind limb osteoblasts (HLOBs), respectively.

3.3. Mandible osteoblasts form more bone than hind limb osteoblasts *in vivo*

To further confirm the osteoblastic characteristics of MaOBs and HLOBs, these cells were implanted together with gelatin scaffolds (ossicles) subcutaneously into C57BL6/J mice, and the ossicles were allowed to grow *in vivo* for 7 weeks. Radiographs of the resulting ossicles revealed that the MaOB seeded ossicles had more mineralization than HLOB seeded ossicles (Fig. 4A&B). The ossicles were decalcified and cryosectioned in order to perform immunofluores-

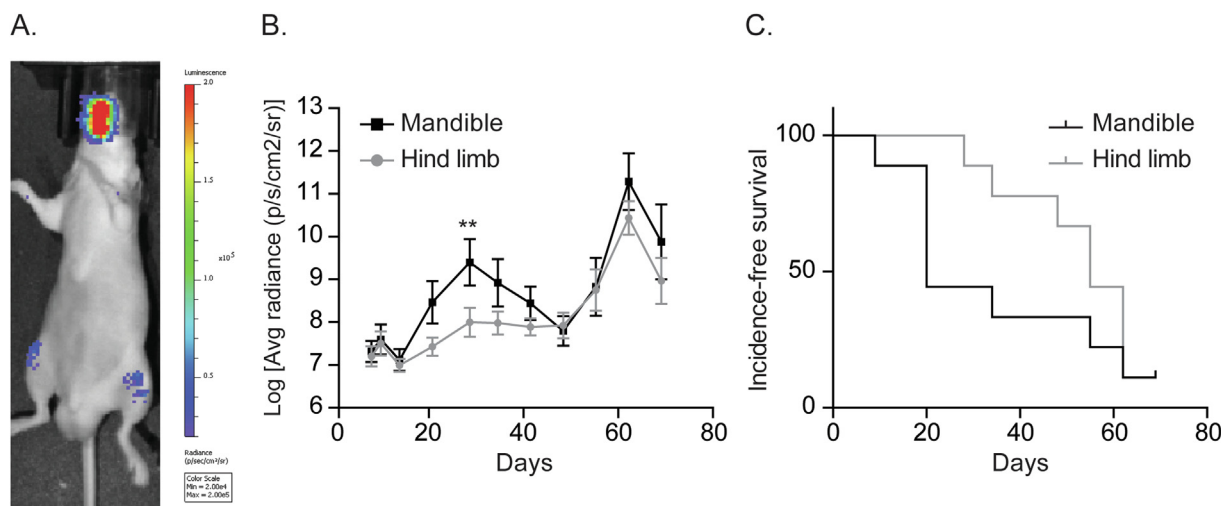


Fig. 1. Metastasis to mandible occurs first after intracardiac injection of PCa cells. Five-week old male nude mice were injected intracardially with 1×10^6 DU145-GFP-luc cells ($n=8$) and observed with bioluminescent imaging (BLI) for 10 weeks. (A) Representative image of a mouse at day 29 demonstrating brighter signal in the mandible than the hindlimbs. (B) All collected longitudinal BLI data after log transformation. Results displayed as Mean \pm SEM. Mixed effects model. $p \leq 0.01$. (C) A 75% cut-off was employed to examine metastasis-free survival (mandible vs. hind limb). Cox proportional hazards model with robust sandwich estimates.

cence for Osteocalcin, hematoxylin and eosin (H&E) staining, and immunohistochemistry for Ki67 (Fig. 4C-E). In order to test whether the cells contained in the ossicles were still osteoblasts, immunofluorescence was performed on the cryosections for Osteocalcin. It is clear that the cells located near and on bone nodules in the ossicles remained Osteocalcin positive, and substantial Osteocalcin appeared to be deposited within the bone itself (Fig. 4C). H&E staining confirmed what was seen by radiograph, as evidenced by increased frequency of woven bone nodules in the MaOB seeded ossicles (Fig. 4D). Visiopharm software was used to automatically quantify tissue section area, and Ki67 positive and negative nuclei. MaOB seeded ossicles were no larger in area than HLOB ossicles (Fig. 4F), but contained a significantly greater number of total and proliferating cells, as evidenced by Ki67 nuclear positivity (Fig. 4G&H).

A possible explanation for the increased proliferation of MaOB cells *in vivo* could be increased vascularity of the MaOB ossicles due to higher levels of VEGF. Interestingly, we did observe greater immunostaining for the endothelial cell markers Endomucin and CD31 in the tissue surrounding and within the implants seeded with MaOBs, when compared to those seeded with HLOBs (Fig. 5A). Still, vascularity of all the implants appeared somewhat scarce and could explain why relative levels of bone formation in the implants appeared lower than other models which use bone marrow stromal cells as the inoculum for ossicle models of bone formation [15]. We also performed immunofluorescence for VEGF using ossicle cryosections as we found differential expression of *Vegfa* in our cell cultures *in vitro* (Fig. 2D). Strangely, we did not see VEGF staining in Osteocalcin positive MaOBs within the implants. However, we did detect VEGF near Osteocalcin positive MaOBs (Fig. 5B), but not HLOBs (data not shown). These results suggest that MaOBs seeded in ossicles may secrete VEGF to the tissues surrounding the implant.

3.4. Mandible osteoblasts support prostate cancer growth more than hind limb osteoblasts *in vitro* and *in vivo*

Our next attempt was then to determine whether there are differential effects between MaOBs and HLOBs on PCa growth. To address this question, human PCa cell lines PC3-GFP-luc and DU145-GFP-luc cells were seeded on top of MaOB or HLOB cells. After 3-5 days of co-culture, more PCa cells were observed on

MaOBs than HLOBs using BLI (Fig. 6A&B). However, L-Ascorbic acid and β -Glycerophosphate supplement failed to induce further tumor proliferation (Fig. 6A&B), suggesting that osteoblastic mineralization was not the major cause of greater PCa proliferation mediated by MaOBs. Then, the changes in the relative amounts of viable cells during *in vitro* culture between MaOBs and HLOBs were compared. As previously reported in rat and human bones [10,11], the cultures containing MaOBs had more viable cells compared to those containing HLOBs (Fig. 6C), suggesting that MaOBs grew significantly faster than HLOBs. However, when mitomycin-C growth arrested MC3T3-E1 cells were cocultured using the same methods, PCa cells actually grew faster on top of growth arrested osteoblasts (Fig. 6D&E). These data suggest that the differences between PCa growth in culture with MaOBs vs. HLOBs are not likely due to baseline differences in mineralization or proliferation.

Next, DU145-GFP-luc cells were co-implanted with either MaOB or HLOB ossicles subcutaneously into athymic nude mice. Similar to what was seen *in vitro*, the growth of DU145-GFP-luc cells co-implanted with MaOB ossicles, as evidenced by significantly brighter BLI signals on the last five measurements, appeared to be greater than those co-implanted with HLOB ossicles (Fig. 7A&B). These results were significantly different despite the fact that one mouse had a much smaller MaOB co-implant tumor than the other four mice (Fig. 8A). With such a limited group size, this tumor cannot be considered an outlier, but it is the reason why the differences observed in the longitudinal data also seem limited (Fig. 7A&B). Sub-analysis of the same data was performed to compare incidence-free survivals, as measured with a 75% signal cut off, and tumors in the MaOB ossicles occurred significantly sooner than in the HLOB ossicles (Fig. 7C). These differences were consistent with *ex vivo* BLI analyses performed on the dissected tumors which again showed significantly brighter signal in the MaOB ossicles (Fig. 7D). As before, radiographs revealed that the MaOB seeded ossicles had more calcification than HLOB seeded ossicles (Fig. 8A&B). In order to test the composition of the cells contained in the co-implanted ossicles, immunofluorescence for pancytokeratin was performed on the cryosections of decalcified ossicles. Clearly, the implants with both MaOBs and HLOBs at 20 weeks contained PCa tumor cells (Fig. 8C). H&E staining and immunohistochemistry for Ki67 were also performed on the co-implanted ossicles to further determine their morphology and cell proliferation status (Fig. 8D&E). Visiopharm software was used to auto-

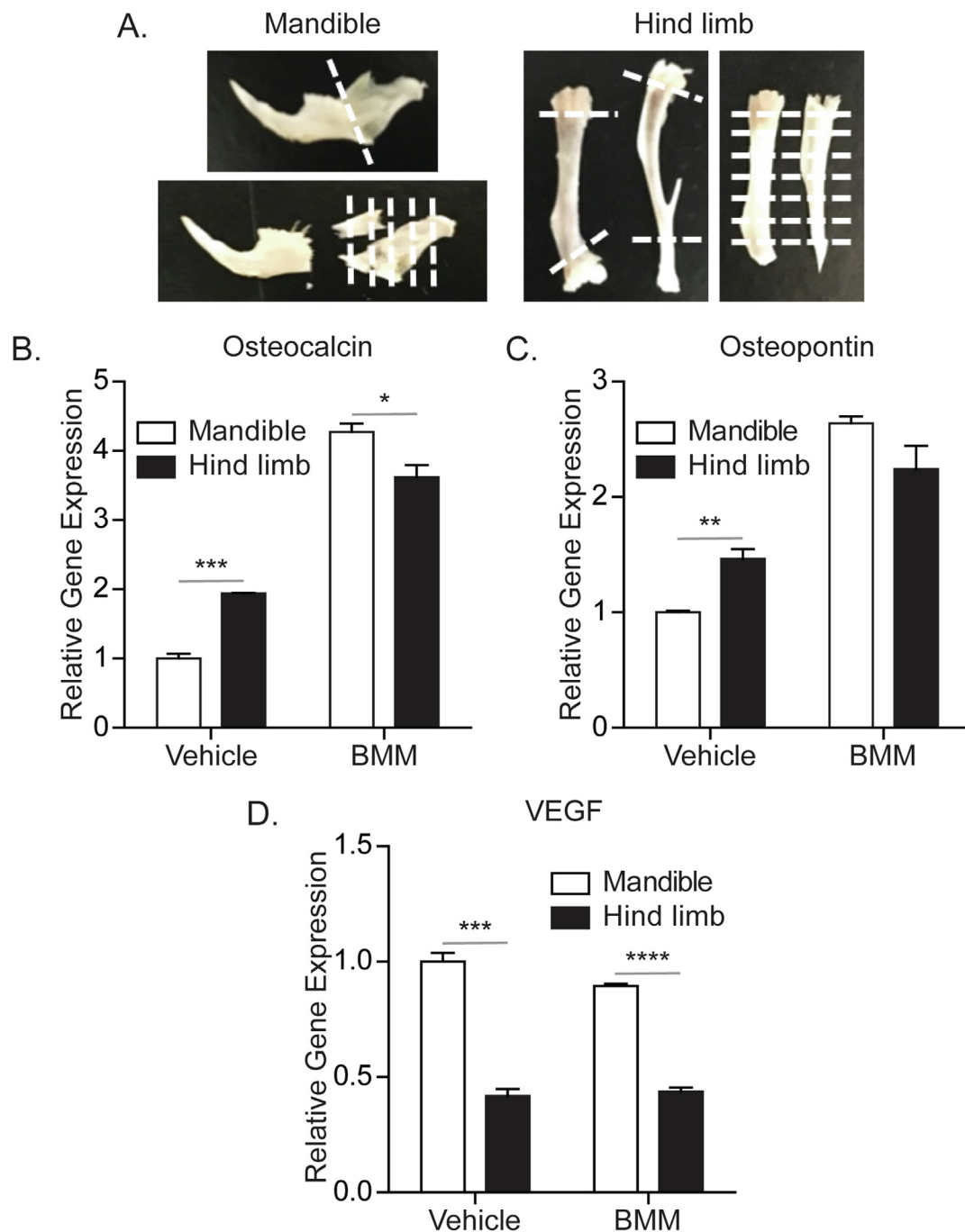


Fig. 2. Cells harvested from mandible and hind limb bones express osteoblast markers. Five-week old male C57BL6/J mice were euthanized, and mandibles and hind limbs were harvested. Mandible and hind limb cells were cultured with bone mineralization medium (BMM) (0.5mM L-Ascorbic acid, 2mM β -Glycerophosphate disodium salt hydrate, and 10mM HEPES) or vehicle (10mM HEPES) for 10 days. (A) Schematic of bone culture preparation: molars, incisors and dental pulp of the mandibles were removed and discarded; epiphyses from the femurs and tibias were cut and the marrow was removed by centrifugation; remaining pieces of the mandibles and femurs/tibias were minced into smaller pieces, digested with trypsin, and cultured and expanded for two weeks before experiments. (B) Relative gene expression of Osteocalcin (Bglap), normalized to vehicle treated mandible cell cultures. (C) Relative gene expression of Osteopontin (Spp1), normalized to vehicle treated mandible cell cultures. (D) Relative gene expression of vascular endothelial growth factor (VEGF), normalized to vehicle treated mandible cell cultures. Gapdh was used as reference gene. Delta-delta Ct method. Results displayed as Mean \pm SEM. Unpaired Student's *t*-test. **p* \leq 0.05, ***p* \leq 0.01, ****p* \leq 0.001, *****p* \leq 0.0001.

matically quantify tissue section area, and Ki67 positive and negative nuclei. MaOB seeded ossicles appeared larger in area than HLOB ossicles, although not quite significant (Fig. 8F), but contained a significantly greater number of total and proliferating cells, as evidenced by Ki67 nuclear positivity (Fig. 8G&H).

4. Discussion

In this study, we first demonstrated that in the intracardiac model of metastatic PCa, mandible bone lesions often occur before hind limb bone lesions, which is anecdotally well-recognized. We

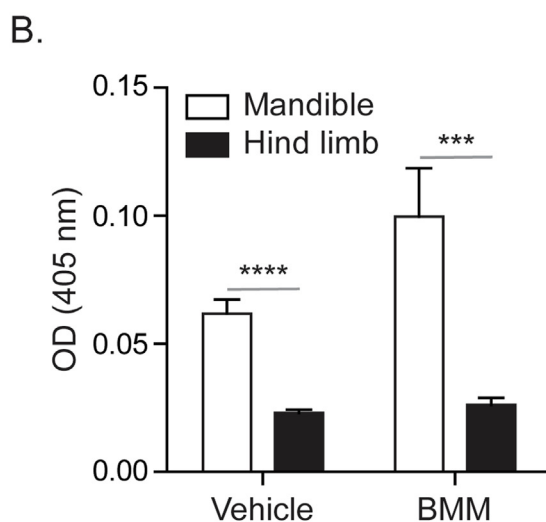
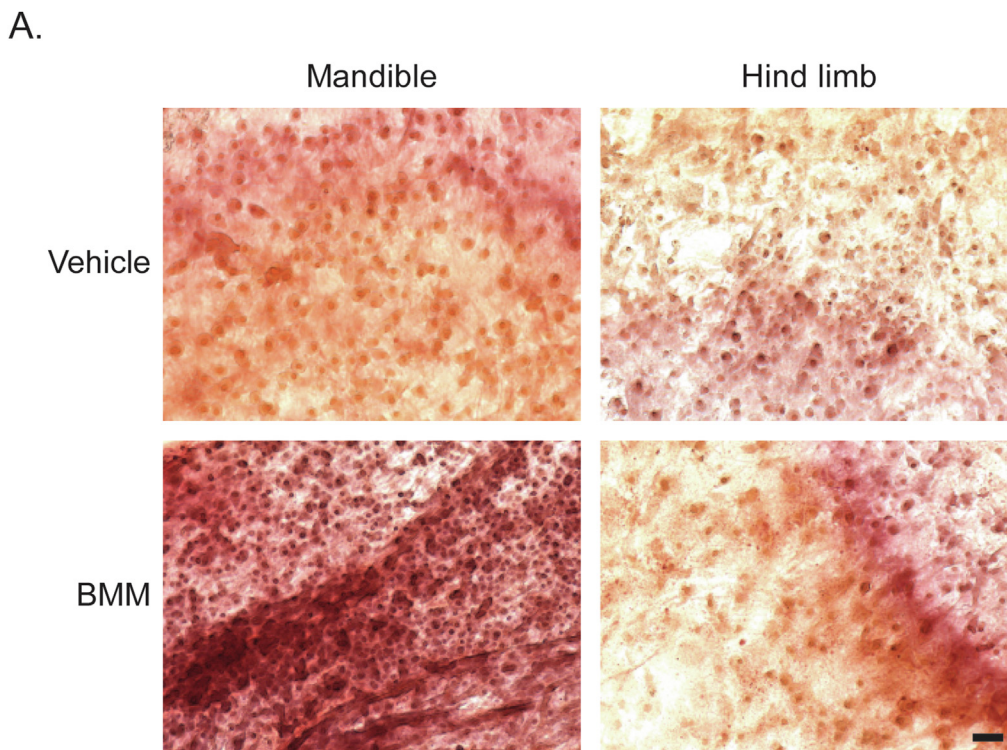


Fig. 3. Cells harvested from mandibles mineralize more than those from hind limbs. Mandible and hind limb cells were cultured with bone mineralization medium (BMM) (0.5mM L-Ascorbic acid, 2mM β-Glycerophosphate disodium salt hydrate, and 10mM HEPES) or vehicle (10mM HEPES) for 14 days. Cells were stained with 2% Alizarin Red S. (A) Representative Alizarin Red S image. Magnification 10x. Bar = 50 μm. (B) Residual stain from whole plates were extracted with acetic acid and read at 405 nm on a plate reader. Results displayed as Mean ± SEM. Unpaired Student's t-test. ****p* ≤ 0.001, *****p* ≤ 0.0001.

showed that cells derived from both the mandible and hind limb bones of mice have osteoblastic properties, and that MaOBs have a higher potential for osteoblastic differentiation than HLOBs both *in vitro* and *in vivo*. Interestingly, when PCa cells were co-cultured with these osteoblasts, PCa cells grew significantly faster in co-culture with MaOBs compared to HLOBs. Consistently, PCa cells co-implanted with MaOBs into animals grew faster and larger tumors than those co-implanted with HLOBs. Altogether, the data suggest that these differences may not be due to differences in mineralization status, as L-Ascorbic acid and β-Glycerophosphate supplementation failed to increase PCa growth *in vitro*, nor differ-

ences in osteoblast proliferation, as mitomycin-C growth arrest of osteoblasts actually increased PCa growth *in vitro*. However, the observations that MaOBs vascularize more *in vivo* and express significantly higher levels of *Vegfa* *in vitro* may be clues to a possible mechanism, although careful mechanistic studies must be performed in order to investigate this further.

The idea that there are different subpopulations of osteoblasts that exhibit different functions in the bone microenvironment has been discussed. For example, while mature osteoblasts form mineral deposits by differentiating osteocytes in healthy bone during homeostasis [24], immature osteoblasts are involved in the

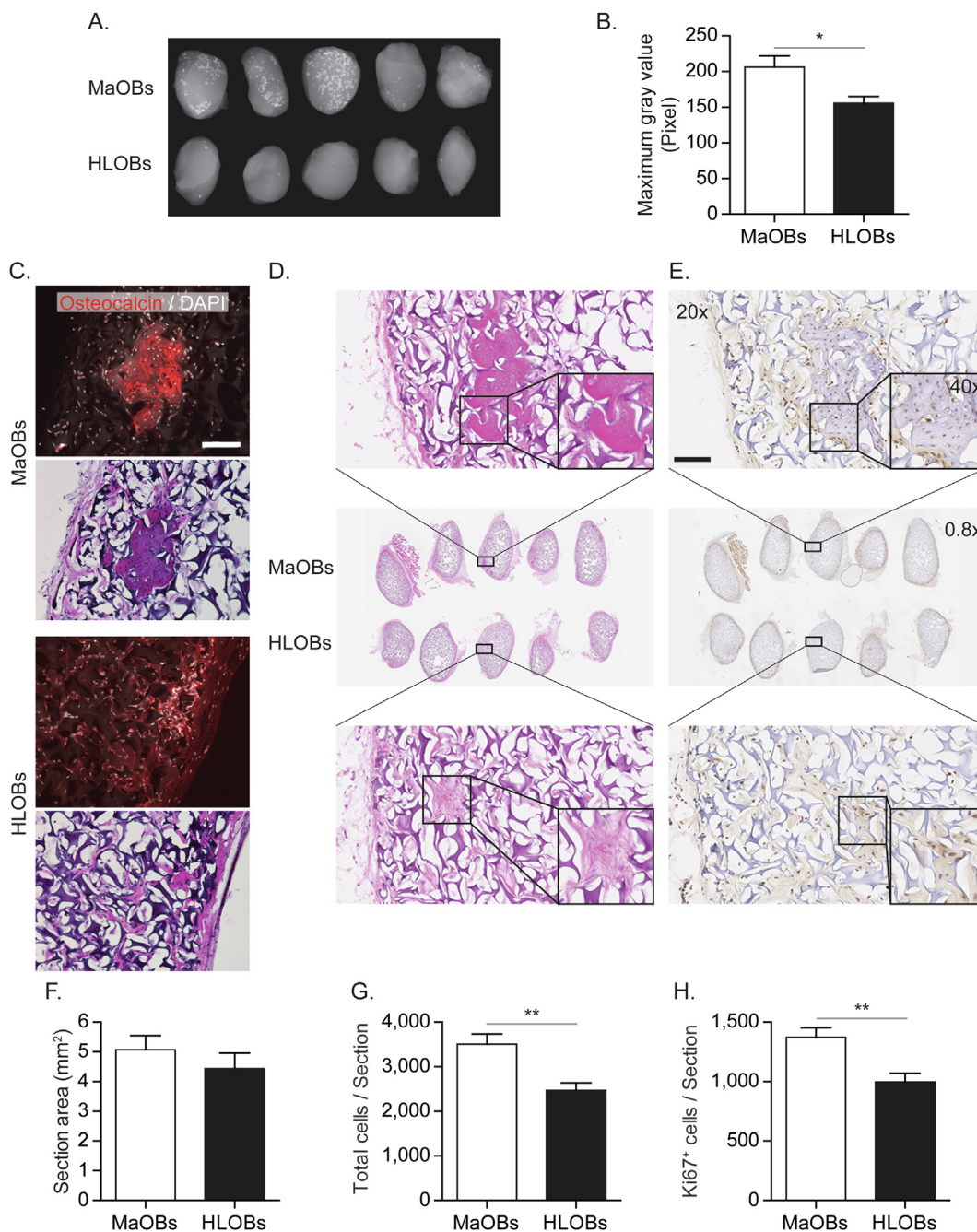


Fig. 4. Cells harvested from mandibles are more proliferative and form more bone than from hind limbs. 1×10^6 primary cells (MaOBs or HLOBs) were seeded onto absorbable gelatin sponges and implanted into subcutaneous pouches of 5-week old male C57BL6/J mice (n=5) and grown for 7 weeks *in vivo*. (A) After euthanasia, implants were dissected, fixed, and radiographed. (B) Densitometry quantification using ImageJ of (A). (C) Representative osteocalcin immunofluorescence and H&E image of (A). DAPI was used for nuclear staining. Magnification 20x. Bar = 100 μ m. (D) Representative H&E image of (A). Bar = 100 μ m. (E) Representative Ki67 immunohistochemical image of (A). Bar = 100 μ m. (F-H) Automated quantification using Visiopharm software of (F) tissue section area, (G) total cells per tissue section, and (H) Ki67 nuclear positive cells per tissue section. Results displayed as Mean \pm SEM. Paired Student's *t*-test. **p* \leq 0.05, ***p* \leq 0.01.

process of bone resorption by activating osteoclasts through the production of receptor activator of NF- κ B ligand (RANKL) [25,26]. In fact, when we tested relative gene expression of RANKL, we found that MaOBs express higher levels than HLOBs (1.00 ± 0.023 vs 0.097 ± 0.021), although they also expressed higher levels of osteoprotegerin (1.00 ± 0.12 vs 0.29 ± 0.014). Osteoprotegerin is a molecule that binds RANKL, inhibiting its ability to activate its receptor RANK on osteoclasts [27]. Similarly, intercellular adhesion molecule (ICAM)-1 positive osteoblasts, which are in G0/G1 phase of the cell cycle arrest, contributed more to osteoclastogenesis than

bone formation, by interacting with monocytes [28]. This phenomenon is also known in the process of hematopoiesis. It has been demonstrated that the activated leukocyte cell adhesion molecule (ALCAM) positive/Sca-1 negative immature osteoblasts are responsible for maintenance of long-term reconstitution activity of HSCs [29]. On the other hand, it has been suggested that the major function of mature osteoblasts is to control the maintenance of lymphoid progenitors, but not hematopoietic stem cells or myeloid progenitors [30]. Moreover, it has been recently revealed that specific subpopulations of osteoblasts influence bone

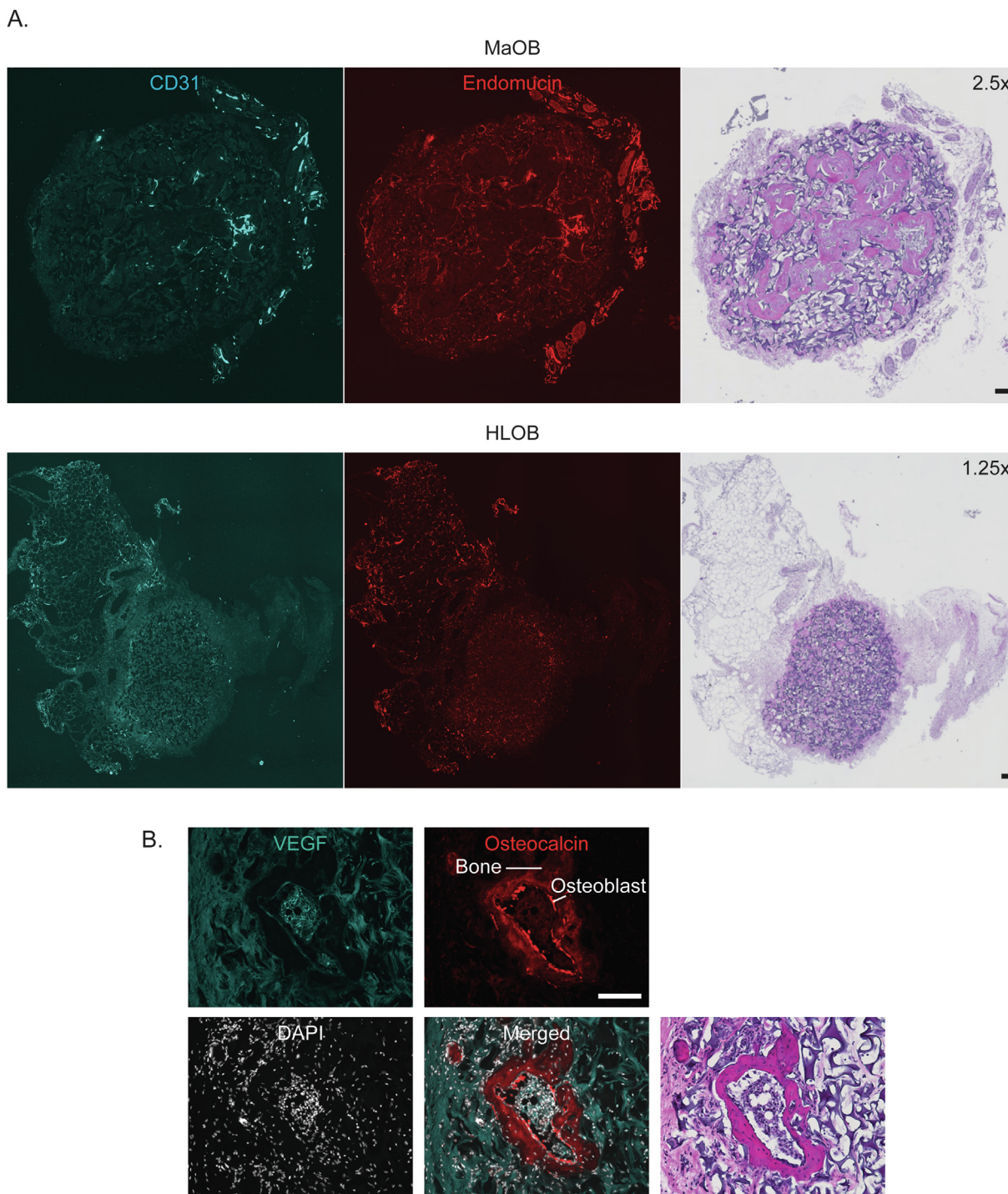


Fig. 5. Ossicle vascularity is mainly localized to tissue surrounding implant. Immunofluorescence was performed on cryosections from Fig. 4 to assess ossicle vascularity. (A) Representative CD31 and Endomucin staining, and H&E image. DAPI was used for nuclear staining. Magnification 10×. Bar = 100 μm. (B) Representative vascular endothelial growth factor (VEGF) and Osteocalcin immunofluorescence, and H&E image. DAPI was used for nuclear staining. Magnification 20×. Bar = 100 μm.

metastatic progression in the tumor microenvironment. Osteoblast progenitors, but not differentiated or mature osteoblasts, were shown to promote breast cancer cell migration through the release of hepatocyte growth factor (HGF), suggesting that the immature osteoblasts are involved in the early steps of the bone seeding process [31]. When osteoblasts interact with breast cancer cells, they are transformed into OPN positive/interleukin (IL)-6 negative/ α -smooth muscle actin (SMA) negative osteoblasts [12]. When these cancer-associated osteoblasts were co-cultured with breast cancer

cells, the growth of breast cancer cells was significantly suppressed and the expression of the cell cycle arrest marker p21 was activated [12].

To investigate the specific effect of osteoblasts on bone metastatic growth of PCa, we took a simplified approach, by focusing solely on the osteoblast component of the bone-metastatic tumor microenvironment. This is an obvious limitation of this study, as there are many cell types other than osteoblasts that exist in the marrow, and these cells are also known to contribute to tumor

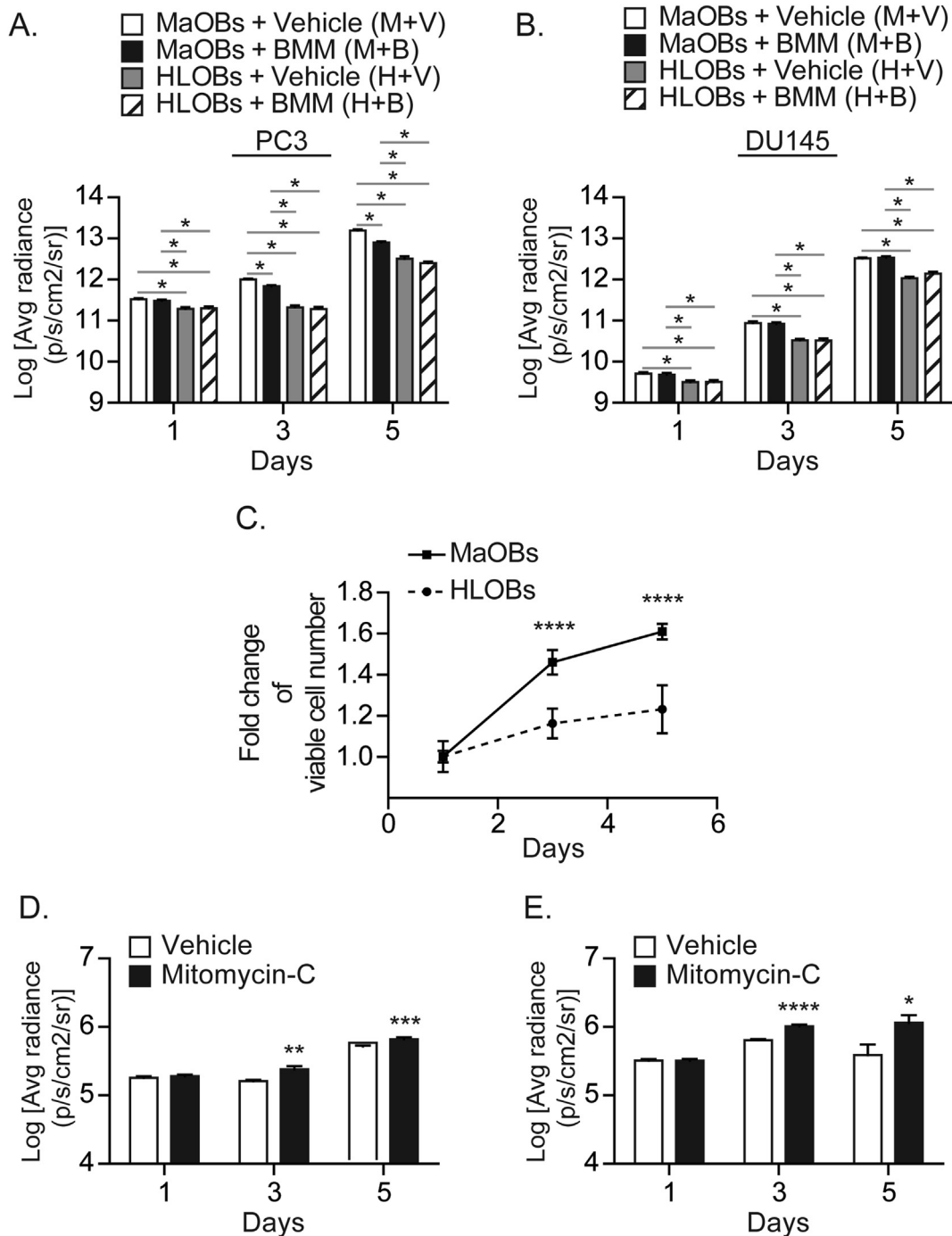


Fig. 6. PCa cells grow faster on osteoblasts harvested from mandibles than osteoblasts from hind limbs. (A) PC3-GFP-luc and (B) DU145-GFP-luc human prostate cancer cells were seeded on top of the primary cells (MaOBs or HLOBs) at a 1:10 ratio. Co-cultures were treated with bone mineralization medium (BMM) (0.5mM L-Ascorbic acid, 2mM β -Glycerophosphate disodium salt hydrate, and 10mM HEPES) or vehicle (10mM HEPES) for 5 days. Bioluminescent imaging (BLI) was measured at day 1, 3, and 5. Two-way ANOVA with Tukey's Studentized Range (HSD) Test for multiple comparisons. (C) MaOBs and HLOBs were seeded in multi-well plates and analyzed for cell proliferation after 1, 3, and 5 days of culture by MTT assay. Proliferation displayed as fold change normalized to day 1. Mixed effects models. (D) PC3-GFP-luc and (E) DU145-GFP-luc human prostate cancer cells were seeded on top of the MC3T3-E1 cells at a 1:10 ratio. To induce cell growth arrest, the MC3T3-E1 cells were pre-treated with vehicle or 10 μ g/mL mitomycin-C for 2.5 h prior to co-culture. BLI was measured at day 1, 3, and 5. Paired Student's *t*-test. Results displayed as Mean \pm SEM. **p* \leq 0.05, ***p* \leq 0.01, ****p* \leq 0.001, *****p* \leq 0.0001.

growth, homeostasis, or dormancy [32]. Although further study is clearly needed, this may be part of the reason why osteoblasts failed to express VEGF during differentiation within the ossicles. Additionally, osteoblasts are not the only cells responsible for general bone health. We believe this is a major reason that we did not observe as robust bone formation as others have reported in their ossicle models of bone marrow stromal cell or mesenchymal stem

cell implantation [10,11]. We believe that in the absence of other stromal cells, the VEGF and other growth factors such as RANKL released by osteoblasts are less effective at promoting angiogenesis and general bone health in an implant model. For instance, osteoblast-derived VEGF has been shown to promote bone formation in a paracrine fashion (which might explain why MaOB ossicles formed more bone than HLOB ossicles in this study), but was

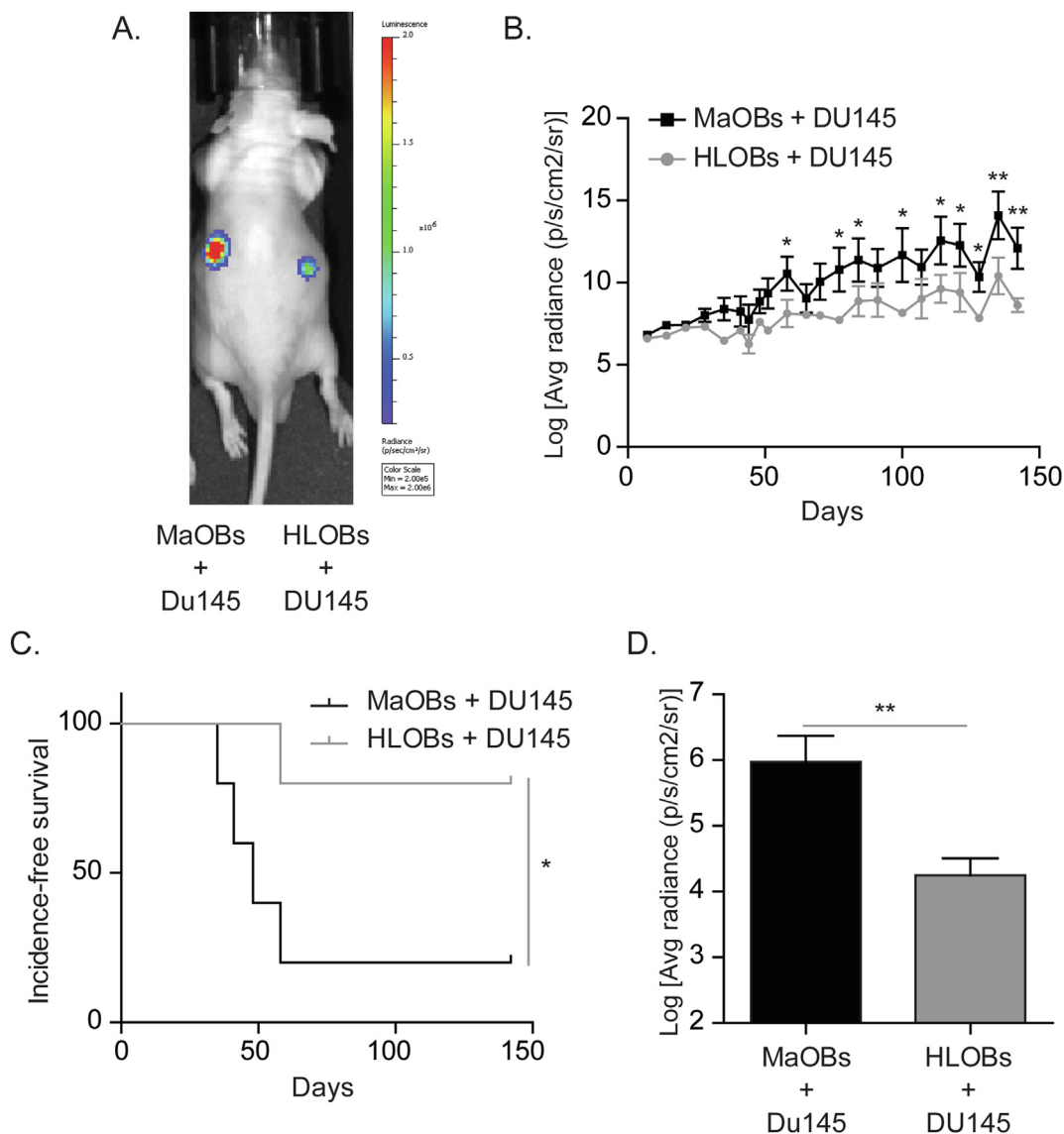


Fig. 7. PCa cells grow faster *in vivo* co-implanted with mandible bone cells. 1×10^6 primary cells (MaOBs or HLOBs) were seeded onto absorbable gelatin sponges and co-implanted into subcutaneous pouches of 5-week old male athymic nude mice ($n=5$) with 1×10^5 DU145-GFP-luc cells and grown for 20 weeks *in vivo*. (A) Representative bioluminescent imaging (BLI) at 20 weeks. (B) All collected longitudinal BLI data after log transformation. Results displayed as Mean \pm SEM. Mixed effects model. (C) 75% cut-off was employed to examine incidence-free survival (MaOBs vs. HLOBs). Cox proportional hazards model with robust sandwich estimates. (D) After euthanasia, tumors were dissected and *ex vivo* BLI performed. Results displayed as Mean \pm SEM. Paired Student's *t*-test. * $p \leq 0.05$, ** $p \leq 0.01$.

also shown to recruit endothelial cells, macrophages, and promote osteoclastogenesis [22]. Further studies to reveal the effects of not only osteoblasts, but also the stroma, endothelium, nerves, osteocytes, osteoclasts, immune cells, and hematopoietic and mesenchymal stem cells on bone and tumor physiology are clearly warranted. The strength of our study is in the *in vivo* co-implant model, which demonstrated that MaOBs contributed to faster tumor cell proliferation than HLOBs. Although the mechanisms behind these differences remain uncertain, the observation that MaOBs promoted greater vascularization *in vivo* could serve as a foundation for further studies. Another finding deserving of future studies was the increased gene expression of RANKL and OPG in MaOBs, as we were also able to detect RANK gene expression in DU145 cells (32.2 ± 1.2 mean cycle threshold; and GAPDH: 26.3 ± 1.1 mean cycle threshold). This finding may help to inform future investigations into mouse mandible tumor frequency, as the question regarding possible differences in tissue seeding and tumor cell anchorage following intracardiac injection remains, and RANKL has

previously been implicated in the bone-metastatic process [33]. Altogether, we believe that these culture methods will be valuable tools in further investigating the mechanisms of tumor cell proliferation in the bone and discovering new interventions to manipulate osteoblast proliferation, activity, or growth factor signaling, which may improve the susceptibility of PCa cells to existing cytotoxic treatments, including chemotherapies.

The findings of this study can be interpreted through the lens of existing treatments used to treat bone metastatic PCa. Current established treatments for bone metastases mainly target bone remodeling, specifically resorption, but these have only had modest success so far, namely denosumab (a human monoclonal antibody against RANKL) and bisphosphonates, which suppress osteoclast activity. Osteoclasts promote bone resorption, creating sufficient space for osteolytic bone tumors to expand and grow [34]. Denosumab and bisphosphonates antagonize bone resorption and as such were hypothesized to slow tumor growth. However, both treatments ultimately fail to improve overall survival

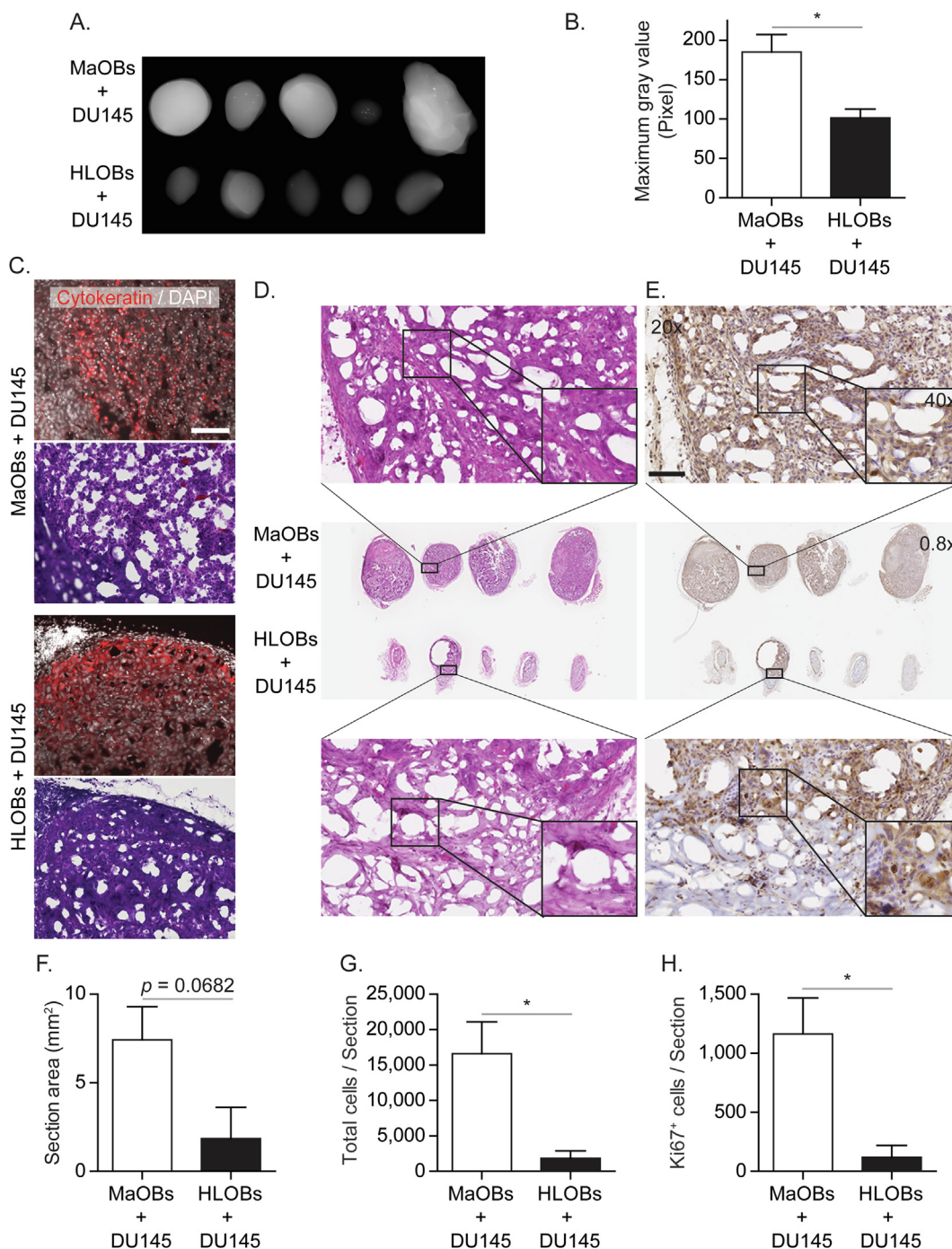


Fig. 8. Tumors from PCa/mandible bone cell co-cultures are more proliferative. (A) After euthanasia, tumors from Fig. 6 were dissected, fixed, and radiographed. (B) Densitometry quantification using ImageJ of (A). (C) Representative Pan-cytokeratin immunofluorescence and H&E image of (A). Magnification 20x. Bar = 100 μm. (D) Representative H&E image of (A). Bar = 100 μm. (E) Representative Ki67 immunohistochemical image of (A). Bar = 100 μm. (F-H) Automated quantification using Visiopharm software of (F) tissue section area, (G) total cells per tissue section, and (H) Ki67 nuclear positive cells per tissue section. Results displayed as Mean ± SE. Paired Student's t-test. **p* ≤ 0.05.

[35,36]. On the other hand, radium-223 (Ra²²³), which forms complexes with hydroxyapatite in bone [37–39], can extend overall survival in PCa patients with bone metastases [40], but only by a few months (mean = 3 months). A variety of combinations of therapies [e.g. docetaxel, second generation androgen deprivation therapies (ADTs) such as abiraterone, enzalutamide, or others] have been shown to extend overall survival of metastatic PCa patients [41]. However, when choosing an effective combination strategy for PCa bone metastases, it may be best to avoid ADTs

since they are known to negatively affect bone health [42,43]. Indeed, a recent trial of the combination of abiraterone and Ra²²³ in patients with bone-metastatic PCa not only failed to improve skeletal event-free survival, but it also increased the frequency of bone fractures compared with placebo [44]. Alternatively, the idea of inducing bone formation by enhancing osteoblastic activity as a treatment for bone metastatic disease has recently been appreciated [45,46], as inactive/immature osteoblasts can reduce PCa susceptibility to chemotherapy [47,48]. However, the results of this

study suggest that inducing osteoblastic differentiation may not be the best strategy for treating progressive bone metastatic tumors, as BMM treatments failed to increase PCa growth in co-culture models. A popular strategy to treat many cancers has been to use drugs that inhibit angiogenesis, but this strategy has been somewhat unsuccessful in the treatment of bone-metastatic PCa [49,50]. This may be in part because these inhibitors mainly target the receptor for VEGF, but not VEGF itself. Here, we see that high *Vegfa* expressing, fast growing, and bone forming MaOBs induced more tumor growth *in vivo* than HLOBs, which expressed less *Vegfa in vitro*, are slower growing, and form less bone *in vivo*. More studies are clearly necessary to elucidate whether osteoblast-derived VEGF, or other angiogenic factors, is required for the faster tumor growth observed in the mandibles of intracardially-injected mice, whether osteoblast-derived VEGF can be targeted to treat bone metastatic disease, and ultimately whether these findings correspond with bone metastatic PCa in humans. We believe that the models described here are valuable tools to aid in this research.

Author contributions

Matthew R. Eber and Yusuke Shiozawa wrote the manuscript with input from all authors. Matthew R. Eber and Yusuke Shiozawa designed study and contributed to data interpretation. Matthew R. Eber, Sun H. Park, Kelly F. Contino, and Chirayu M. Patel performed *in vitro* and *in vivo* experiments. Fang-Chi Hsu performed statistical analyses. Yusuke Shiozawa supervised the study. All authors reviewed and approved the final manuscript.

CRedit authorship contribution statement

Matthew R. Eber: Conceptualization, Data curation, Investigation, Methodology, Writing - original draft, Writing - review & editing. **Sun H. Park:** Data curation, Investigation, Methodology, Writing - review & editing. **Kelly F. Contino:** Data curation, Investigation, Writing - review & editing. **Chirayu M. Patel:** Data curation, Investigation, Writing - review & editing. **Fang-Chi Hsu:** Formal analysis, Methodology, Software, Writing - review & editing. **Yusuke Shiozawa:** Conceptualization, Funding acquisition, Methodology, Project administration, Resources, Supervision, Writing - original draft, Writing - review & editing.

Declaration of Competing Interest

Yusuke Shiozawa has received research funding from TEVA Pharmaceuticals, but not relevant to this study. The remaining authors declare that they have no known competing financial interests or personal relationships that could have appeared to influence the work reported in this paper.

Acknowledgements

This work is directly supported by the National Cancer Institute (R01-CA238888, Y.S.; R44-CA203184, Y.S.), the Department of Defense (W81XWH-14-1-0403, Y.S.; W81XWH-17-1-0541, Y.S.; W81XWH-19-1-0045, Y.S.), METAvivor (METAvivor Research Award, Y.S.), and the Wake Forest Baptist Comprehensive Cancer Center Internal Pilot Funding (Y.S.). This work is also supported by the National Cancer Institute's Cancer Center Support Grant award number P30-CA012197 issued to the Wake Forest Baptist Comprehensive Cancer Center. The authors wish to acknowledge the support of the Wake Forest Baptist Comprehensive Cancer Center Cell Engineering Shared Resource and Flow Cytometry Shared Resource, supported by the National Cancer Institute's Cancer Center Support Grant award number P30-CA012197. The content is

solely the responsibility of the authors and does not necessarily represent the official views of the National Cancer Institute.

References

- [1] Y. Shiozawa, E.A. Pedersen, A.M. Havens, Y. Jung, A. Mishra, J. Joseph, J.K. Kim, L. R. Patel, C. Ying, A.M. Ziegler, M.J. Pienta, J. Song, J. Wang, R.D. Loberg, P.H. Krebsbach, K.J. Pienta, R.S. Taichman, Human prostate cancer metastases target the hematopoietic stem cell niche to establish footholds in mouse bone marrow, *J. Clin. Invest.* 121 (4) (2011) 1298–1312.
- [2] Y. Shiozawa, R.S. Taichman, Getting blood from bone: an emerging understanding of the role that osteoblasts play in regulating hematopoietic stem cells within their niche, *Exp. Hematol.* 40 (9) (2012) 685–694.
- [3] L.M. Calvi, G.B. Adams, K.W. Weibrecht, J.M. Weber, D.P. Olson, M.C. Knight, R. P. Martin, E. Schipani, P. Divieti, F.R. Bringhurst, L.A. Milner, H.M. Kronenberg, D.T. Scadden, Osteoblastic cells regulate the haematopoietic stem cell niche, *Nature* 425 (6960) (2003) 841–846.
- [4] F. Arai, A. Hirao, M. Ohmura, H. Sato, S. Matsuoka, K. Takubo, K. Ito, G.Y. Koh, T. Suda, Tie2/angiopoietin-1 signaling regulates hematopoietic stem cell quiescence in the bone marrow niche, *Cell* 118 (2) (2004) 149–161.
- [5] J. Zhang, C. Niu, L. Ye, H. Huang, X. He, W.G. Tong, J. Ross, J. Haug, T. Johnson, J. Q. Feng, S. Harris, L.M. Wiedemann, Y. Mishina, L. Li, Identification of the haematopoietic stem cell niche and control of the niche size, *Nature* 425 (6960) (2003) 836–841.
- [6] H. Wang, C. Yu, X. Gao, T. Welte, A.M. Muscarella, L. Tian, H. Zhao, Z. Zhao, S. Du, J. Tao, B. Lee, T.F. Westbrook, S.T. Wong, X. Jin, J.M. Rosen, C.K. Osborne, X. H. Zhang, The osteogenic niche promotes early-stage bone colonization of disseminated breast cancer cells, *Cancer Cell* 27 (2) (2015) 193–210.
- [7] Y. Shiozawa, J.E. Berry, M.R. Eber, Y. Jung, K. Yumoto, F.C. Cackowski, H.J. Yoon, P. Parsana, R. Mehra, J. Wang, S. McGee, E. Lee, S. Nagrath, K.J. Pienta, R.S. Taichman, The marrow niche controls the cancer stem cell phenotype of disseminated prostate cancer, *Oncotarget* 7 (27) (2016) 41217–41232.
- [8] F. Arguello, R.B. Baggs, C.N. Frantz, A murine model of experimental metastasis to bone and bone marrow, *Cancer Res.* 48 (23) (1988) 6876–6881.
- [9] Y.T. Qiu, C. Yang, M.J. Chen, W.L. Qiu, Metastatic spread to the mandibular condyle as initial clinical presentation: radiographic diagnosis and surgical experience, *J. Oral Maxillofac. Surg.* 71 (4) (2013) 809–820.
- [10] T.L. Aghaloo, T. Chaichanasakul, O. Bezouglaia, B. Kang, R. Franco, S.M. Dry, E. Atti, S. Tetradis, Osteogenic potential of mandibular vs. long-bone marrow stromal cells, *J. Dent. Res.* 89 (11) (2010) 1293–1298.
- [11] S.O. Akintoye, T. Lam, S. Shi, J. Brahim, M.T. Collins, P.G. Robey, Skeletal site-specific characterization of orofacial and iliac crest human bone marrow stromal cells in same individuals, *Bone* 38 (6) (2006) 758–768.
- [12] A.D. Kolb, A.B. Shupp, D. Mukhopadhyay, F.C. Marini, K.M. Bussard, Osteoblasts are “educated” by crosstalk with metastatic breast cancer cells in the bone tumor microenvironment, *Breast Cancer Res.* 21 (1) (2019) 31.
- [13] S.H. Park, M.R. Eber, Y. Shiozawa, Models of Prostate Cancer Bone Metastasis, *Methods Mol. Biol.* 2019 (1914) 295–308.
- [14] S.R. Amend K.C. Valkenburg K.J. Pienta Murine Hind Limb Long Bone Dissection and Bone Marrow Isolation *J. Vis. Exp.* (110) (2016).
- [15] G.J. Pettway, L.K. McCauley, Ossicle and vossicle implant model systems, *Methods Mol. Biol.* 455 (2008) 101–110.
- [16] C.A. Gregory, W.G. Gunn, A. Peister, D.J. Prockop, An Alizarin red-based assay of mineralization by adherent cells in culture: comparison with cetylpyridinium chloride extraction, *Anal. Biochem.* 329 (1) (2004) 77–84.
- [17] S.H. Park, M.R. Eber, S. Tsuzuki, M.E. Booker, A.G. Sunil, D.B. Widner, R.A. Parker, C.M. Peters, Y. Shiozawa, Adeno-associated virus serotype rh10 is a useful gene transfer vector for sensory nerves that innervate bone in immunodeficient mice, *Sci. Rep.* 7 (1) (2017) 17428.
- [18] A.A. Khalil, M.J. Jameson, W.C. Broadus, P.S. Lin, S.M. Dever, S.E. Golding, E. Rosenberg, K. Valerie, T.D. Chung, The Influence of Hypoxia and pH on Bioluminescence Imaging of Luciferase-Transfected Tumor Cells and Xenografts, *Int. J. Mol. Imaging* 2013 (2013) 287697.
- [19] L.Y. Yu-Lee, Y.C. Lee, J. Pan, S.C. Lin, T. Pan, G. Yu, D.H. Hawke, B.F. Pan, S.H. Lin, Bone secreted factors induce cellular quiescence in prostate cancer cells, *Sci. Rep.* 9 (1) (2019) 18635.
- [20] L.Y. Yu-Lee, G. Yu, Y.C. Lee, S.C. Lin, J. Pan, T. Pan, K.J. Yu, B. Liu, C.J. Creighton, J. Rodriguez-Canales, P.A. Villalobos, E. Wistuba II, F. de Nadal, G.E. Posas, S.H.L. Gallick, Osteoblast-Secreted Factors Mediate Dormancy of Metastatic Prostate Cancer in the Bone via Activation of the TGFbetaRIII-p38MAPK-pS249/T252RB Pathway, *Cancer Res.* 78 (11) (2018) 2911–2924.
- [21] Y. Shiozawa, E.A. Pedersen, L.R. Patel, A.M. Ziegler, A.M. Havens, Y. Jung, J. Wang, S. Zalucha, R.D. Loberg, K.J. Pienta, R.S. Taichman, GAS6/AXL axis regulates prostate cancer invasion, proliferation, and survival in the bone marrow niche, *Neoplasia* 12 (2) (2010) 116–127.
- [22] K. Hu, B.R. Olsen, Osteoblast-derived VEGF regulates osteoblast differentiation and bone formation during bone repair, *J. Clin. Invest.* 126 (2) (2016) 509–526.
- [23] E. Roberts, D.A. Cossigny, G.M. Quan, The role of vascular endothelial growth factor in metastatic prostate cancer to the skeleton, *Prostate Cancer* 2013 (2013) 418340.
- [24] N. Sawa, H. Fujimoto, Y. Sawa, J. Yamashita, Alternating Differentiation and Dedifferentiation between Mature Osteoblasts and Osteocytes, *Sci. Rep.* 9 (1) (2019) 13842.
- [25] H. Li, X. Jiang, J. Delaney, T. Franceschetti, I. Bilic-Curcic, J. Kalinovsky, J.A. Lorenzo, D. Grcevic, D.W. Rowe, I. Kalajzic, Immature osteoblast lineage cells

- increase osteoclastogenesis in osteogenesis imperfecta murine, *Am. J. Pathol.* 176 (5) (2010) 2405–2413.
- [26] G.P. Thomas, S.U. Baker, J.A. Eisman, E.M. Gardiner, Changing RANKL/OPG mRNA expression in differentiating murine primary osteoblasts, *J. Endocrinol.* 170 (2) (2001) 451–460.
- [27] B.F. Boyce, L. Xing, Biology of RANK, RANKL, and osteoprotegerin, *Arthritis Res Ther* 9 (Suppl 1) (2007) S1.
- [28] Y. Tanaka, A. Maruo, K. Fujii, M. Nomi, T. Nakamura, S. Eto, Y. Minami, Intercellular adhesion molecule 1 discriminates functionally different populations of human osteoblasts: characteristic involvement of cell cycle regulators, *J. Bone Miner. Res.* 15 (10) (2000) 1912–1923.
- [29] Y. Nakamura, F. Arai, H. Iwasaki, K. Hosokawa, I. Kobayashi, Y. Gomei, Y. Matsumoto, H. Yoshihara, T. Suda, Isolation and characterization of endosteal niche cell populations that regulate hematopoietic stem cells, *Blood* 116 (9) (2010) 1422–1432.
- [30] L. Ding, S.J. Morrison, Haematopoietic stem cells and early lymphoid progenitors occupy distinct bone marrow niches, *Nature* 495 (7440) (2013) 231–235.
- [31] S. Vallet, M.H. Bashari, F.J. Fan, S. Malvestiti, A. Schneeweiss, P. Wuchter, D. Jager, K. Podar, Pre-Osteoblasts Stimulate Migration of Breast Cancer Cells via the HGF/MET Pathway, *PLoS ONE* 11 (3) (2016) e0150507.
- [32] Y. Shiozawa, M.R. Eber, J.E. Berry, R.S. Taichman, Bone marrow as a metastatic niche for disseminated tumor cells from solid tumors, *Bonekey Rep.* 4 (2015) 689.
- [33] T. Asano, K. Okamoto, Y. Nakai, M. Tsutsumi, R. Muro, A. Suematsu, K. Hashimoto, T. Okamura, S. Ehata, T. Nitta, H. Takayanagi, Soluble RANKL is physiologically dispensable but accelerates tumour metastasis to bone, *Nat. Metab.* 1 (9) (2019) 868–875.
- [34] A. Maurizi, N. Rucci, The Osteoclast in Bone Metastasis: Player and Target, *Cancers (Basel)* 10 (7) (2018).
- [35] A.T. Stopeck, A. Lipton, J.J. Body, G.G. Steger, K. Tonkin, R.H. de Boer, M. Lichinitser, Y. Fujiwara, D.A. Yardley, M. Viniestra, M. Fan, Q. Jiang, R. Dansey, S. Jun, A. Braun, Denosumab compared with zoledronic acid for the treatment of bone metastases in patients with advanced breast cancer: a randomized, double-blind study, *J. Clin. Oncol.* 28 (35) (2010) 5132–5139.
- [36] K. Fizazi, M. Carducci, M. Smith, R. Damiao, J. Brown, L. Karsh, P. Milecki, N. Shore, M. Rader, H. Wang, Q. Jiang, S. Tadros, R. Dansey, C. Goessl, Denosumab versus zoledronic acid for treatment of bone metastases in men with castration-resistant prostate cancer: a randomised, double-blind study, *Lancet* 377 (9768) (2011) 813–822.
- [37] S.K. Badrising, V. van der Noort, P. Hamberg, J.L. Coenen, M.J. Aarts, I.M. van Oort, A.J. van den Eertwegh, M. Los, H.P. van den Berg, H. Gelderblom, S. Vrijaldenhoven, E.D. Kerver, T. van Voorthuizen, I.J. de Jong, J.B. Haanen, A.M. Bergman, Enzalutamide as a Fourth- or Fifth-Line Treatment Option for Metastatic Castration-Resistant Prostate Cancer, *Oncology* 91 (5) (2016) 267–273.
- [38] F. Vignani, V. Bertaglia, C. Buttigliero, M. Tucci, G.V. Scagliotti, M. Di Maio, Skeletal metastases and impact of anticancer and bone-targeted agents in patients with castration-resistant prostate cancer, *Cancer Treat. Rev.* 44 (2016) 61–73.
- [39] D.S. Abou, D. Ulmert, M. Doucet, R.F. Hobbs, R.C. Riddle, D.L. Thorek, Whole-Body and Microenvironmental Localization of Radium-223 in Naive and Mouse Models of Prostate Cancer Metastasis, *J. Natl Cancer Inst.* 108 (5) (2016).
- [40] C. Parker, S. Nilsson, D. Heinrich, S.I. Helle, J.M. O'Sullivan, S.D. Fossa, A. Chodacki, P. Wiechno, J. Logue, M. Seke, A. Widmark, D.C. Johannessen, P. Hoskin, D. Bottomley, N.D. James, A. Solberg, I. Syndikus, J. Kliment, S. Wedel, S. Boehmer, M. Dall'Oglio, L. Franzen, R. Coleman, N.J. Vogelzang, C.G. O'Bryan-Tear, K. Staudacher, J. Garcia-Vargas, M. Shan, O.S. Bruland, O. Sartor, A. Investigators, Alpha emitter radium-223 and survival in metastatic prostate cancer, *N. Engl. J. Med.* 369 (3) (2013) 213–223.
- [41] G. Gravis, Systemic treatment for metastatic prostate cancer, *Asian J. Urol.* 6 (2) (2019) 162–168.
- [42] C.E. Lee, W.D. Leslie, P. Czaykowski, J. Geringerich, M. Geirnaert, Y.K. Lau, A comprehensive bone-health management approach for men with prostate cancer receiving androgen deprivation therapy, *Curr. Oncol.* 18 (4) (2011) e163–e172.
- [43] D.K. Kim, J.Y. Lee, K.J. Kim, N. Hong, J.W. Kim, Y.S. Hah, K.C. Koo, J.H. Kim, K.S. Cho, Effect of Androgen-Deprivation Therapy on Bone Mineral Density in Patients with Prostate Cancer: A Systematic Review and Meta-Analysis, *J. Clin. Med.* 8 (1) (2019).
- [44] M. Smith, C. Parker, F. Saad, K. Miller, B. Tombal, Q.S. Ng, M. Boegemann, V. Matveev, J.M. Piulats, L.E. Zucca, O. Karyakin, G. Kimura, N. Matsubara, W.C. Nahas, F. Nole, E. Rosenbaum, A. Heidenreich, Y. Kakehi, A. Zhang, H. Krissel, M. Teufel, J. Shen, V. Wagner, C. Higano, Addition of radium-223 to abiraterone acetate and prednisone or prednisolone in patients with castration-resistant prostate cancer and bone metastases (ERA 223): a randomised, double-blind, placebo-controlled, phase 3 trial, *Lancet Oncol.* 20 (3) (2019) 408–419.
- [45] E. Hesse, S. Schroder, D. Brandt, J. Pamperin, H. Saito, H. Taipaleenmaki, Sclerostin inhibition alleviates breast cancer-induced bone metastases and muscle weakness, *JCI Insight* 5 (2019).
- [46] D. Toscani, M. Bolzoni, M. Ferretti, C. Palumbo, N. Giuliani, Role of Osteocytes in Myeloma Bone Disease: Anti-sclerostin Antibody as New Therapeutic Strategy, *Front. Immunol.* 9 (2018) 2467.
- [47] H. Zheng, Y. Bae, S. Kasimir-Bauer, R. Tang, J. Chen, G. Ren, M. Yuan, M. Esposito, W. Li, Y. Wei, M. Shen, L. Zhang, N. Tupitsyn, K. Pantel, C. King, J. Sun, J. Moriguchi, H.T. Jun, A. Coxon, B. Lee, Y. Kang, Therapeutic Antibody Targeting Tumor- and Osteoblastic Niche-Derived Jagged1 Sensitizes Bone Metastasis to Chemotherapy, *Cancer Cell* 32(6) (2017) 731–747 e6.
- [48] N. Sethi, X. Dai, C.G. Winter, Y. Kang, Tumor-derived JAGGED1 promotes osteolytic bone metastasis of breast cancer by engaging notch signaling in bone cells, *Cancer Cell* 19 (2) (2011) 192–205.
- [49] A. Spreafico, K.N. Chi, S.S. Sridhar, D.C. Smith, M.A. Carducci, P. Kavsak, T.S. Wong, L. Wang, S.P. Ivy, S.D. Mukherjee, C.K. Kollmannsberger, M.A. Sukhai, N. Takebe, S. Kamel-Reid, L.L. Siu, S.J. Hotte, A randomized phase II study of cediranib alone versus cediranib in combination with dasatinib in docetaxel resistant, castration resistant prostate cancer patients, *Invest. New Drugs* 32 (5) (2014) 1005–1016.
- [50] E. Heath, L. Heilbrun, H. Mannuel, G. Liu, P. Lara, J.P. Monk, T. Flaig, A. Zurita, P. Mack, U. Vaishampayan, P. Stella, D. Smith, S. Bolton, A. Hussain, A. Al-Janadi, D. Silbiger, M. Usman, S.P. Ivy, Phase II, Multicenter, Randomized Trial of Docetaxel plus Prednisone with or Without Cediranib in Men with Chemotherapy-Naive Metastatic Castrate-Resistant Prostate Cancer, *Oncologist* 24 (9) (2019) 1149–e807.